Water Science and Engineering 2023, 16(1): 14−25

HOSTED BY

ELSEVIER

Available online at www.sciencedirect.com

Water Science and Engineering

journal homepage: wse.hhu.edu.cn

Morphodynamic signatures derived from daily surface elevation dynamics can explain the morphodynamic development of tidal flats

Tim J. Grandjean [a,b,*], Jaco C. de Smit [a], Jim van Belzen [a], Gregory S. Fivash [a], Jeroen van Dalen [a], Tom Ysebaert [a], Tjeerd J. Bouma [a,b]

[a] *Department of Estuarine and Delta Systems, Royal Netherlands Institute for Sea Research (NIOZ), 4401 NT Yerseke, The Netherlands*
[b] *Faculty of Geosciences, Department of Physical Geography, Utrecht University, 3508 TC Utrecht, The Netherlands*

Received 31 March 2022; accepted 1 November 2022
Available online 30 November 2022

Abstract

Understanding the sensitivity of tidal flats to environmental changes is challenging. Currently, most studies rely on process-based models to systematically explain the morphodynamic evolution of tidal flats. In this study, we proposed an alternative empirical approach to explore tidal flat dynamics using statistical indices based on long-term time series of daily surface elevation development. Surface elevation dynamic (SED) indices focus on the magnitude and period of surface elevation changes, while morphodynamic signature (MDS) indices relate sediment dynamics to environmental drivers. The statistical analyses were applied to an intervention site in the Netherlands to determine the effect of recently constructed groynes on the tidal flat. Using these analyses, we were able to (1) detect a reduction in the daily SED and (2) determine that the changes in the daily SED were predominantly caused by the reduction in wave impact between the groynes rather than the reduction in tidal currents. Overall, the presented results showed that the combination of novel statistical indices provides new insights into the trajectories of tidal flats, ecosystem functioning, and sensitivity to physical drivers (wind and tides). Finally, we suggested how the SED and MDS indices may help to explore the future trajectories and climate resilience of intertidal habitats.

Keywords: Surface elevation dynamics; Tidal flat trajectories; Morphodynamic development; Morphodynamic signature; Bed level dynamics

1. Introduction

Intertidal habitats, such as salt marshes, mangroves, and unvegetated tidal flats, are among the most widely distributed coastal ecosystems worldwide (Millennium Ecosystem Assessment, 2005). They support the livelihood of coastal communities with essential ecosystem functions and services, such as storm protection through wave attenuation (Temmerman et al., 2013) and shoreline stabilization (Shepard et al., 2011). They are also major habitats for migratory birds and commercially important species (Barbier, 2019). Worldwide, tidal areas are under intense pressure from human-induced changes, such as rising sea levels (Passeri et al., 2015), coastal developments, and reduced sediment fluxes (Li et al., 2014). There is a growing concern about the trajectory of these intertidal habitats as their areas are reducing worldwide (Murray et al., 2019; Goldberg et al., 2020). Although the responses to climate change and rising sea levels for vegetated tidal wetlands are well known (Kirwan and Temmerman, 2009; Fagherazzi et al., 2020; Saintilan et al., 2020), few studies have elucidated the fate of unvegetated "bare" tidal flats.

To date, many analytical (e.g., de Vriend et al., 2011; Wang et al., 2015; de Vet et al., 2017) and numerical modeling (e.g., Le Hir et al., 2000; Hu et al., 2015b; de Vet et al., 2018) studies have focused on the (bio)physical processes shaping

This work was supported by the Royal Netherlands Academy of Arts and Sciences (KNAW) (Grant No. PSA-SA-E-02) and the Province of Zeeland, the Netherlands (Grant No. CoE-Buitendijks).
* Corresponding author.
E-mail address: tim.grandjean@nioz.nl (Tim J. Grandjean).
Peer review under responsibility of Hohai University.

https://doi.org/10.1016/j.wse.2022.11.003

the morphology of tidal flats. Both approaches often use the existence of a dynamic equilibrium to predict large-scale tidal flat morphology (Kirby, 2000; Friedrichs, 2011; van der Wegen and Jaffe, 2014). On shorter timescales, however, tidal flat morphology may deviate from the dynamic equilibrium (Hu et al., 2015b). For example, recent extensive observations have shown that disturbance events can lead to noticeable changes in the morphodynamic development of a tidal flat (Belliard et al., 2019; de Vet et al., 2020). Understanding the perturbation of the dynamic equilibrium is crucial to studies of the biophysical processes of a tidal flat because the daily surface elevation dynamics (SED) on tidal flats drive the recruitment and persistence of benthic organisms (Nambu et al., 2012; Shi et al., 2021), the establishment of vegetation over the tidal flat (Bouma et al., 2016; Cao et al., 2018), and the position and dynamics of the edges of tidal wetlands (Bouma et al., 2016; Willemsen et al., 2018). In other words, young organisms require a period with stable bed level dynamics to germinate and to establish and develop tolerance under harder conditions (Cao et al., 2018; van Belzen et al., 2022). To predict the aforementioned ecological processes, it is necessary to quantify SED rather than understand the hydrodynamics that cause the sediment dynamics (Bouma et al., 2016). Hence, there is a need to capture the daily SED or the short-term variation between accretion and erosion over space and time. To quantify the short-term SED, a high-resolution and low-cost standalone SED sensor was developed at the Royal Netherlands Institute for Sea Research (Hu et al., 2015a, 2021). In recent years, SED sensors have revealed the relation between the hydrodynamics and short-term sediment dynamics of tidal systems. For example, tidal currents dominate the sediment dynamics of the low tidal flat, while the dynamics of the high tidal flat are often a product of wave activity (Belliard et al., 2019). In both low and high tidal flats, however, an individual storm event can impact the surface elevation in a manner comparable to a chronic surface elevation development that takes several years (Hu et al., 2018; de Vet et al., 2020). Thus far, as long-term datasets do not yet exist, SED sensor research has been limited to specific mechanisms over limited timeframes. We aimed to explore whether SED sensor data collected over multiple years can be used to derive more general statistical indices to characterize the morphodynamic behavior of unvegetated tidal flats and to determine whether such indices can be used to predict their medium-term (annual) trajectories.

In this article, we developed a method to analyze daily SED and link them to drivers in order to understand the relation of sediment dynamics to biophysical parameters (Fig. 1). Compared to existing analytical and numerical modeling methods, this method is an alternative approach based on statistical analyses. It characterizes morphodynamic developments (1) by deriving statistical indices from extensive time series of daily SED measurements acquired from SED sensors and (2) by correlating these time series to meteorological and tidal forcing drivers. The first analyses were carried out over several years of daily surface elevation changes to obtain statistical indices relevant to benthic invertebrate settlement and wetland seedling establishment, here expressed as the SED average variability (SED_{var}) and the SED return time (SED_{rt}). Next, two novel statistical relationships in the form of morphodynamic signatures (MDS) were obtained to test the correlations between the daily SED and natural

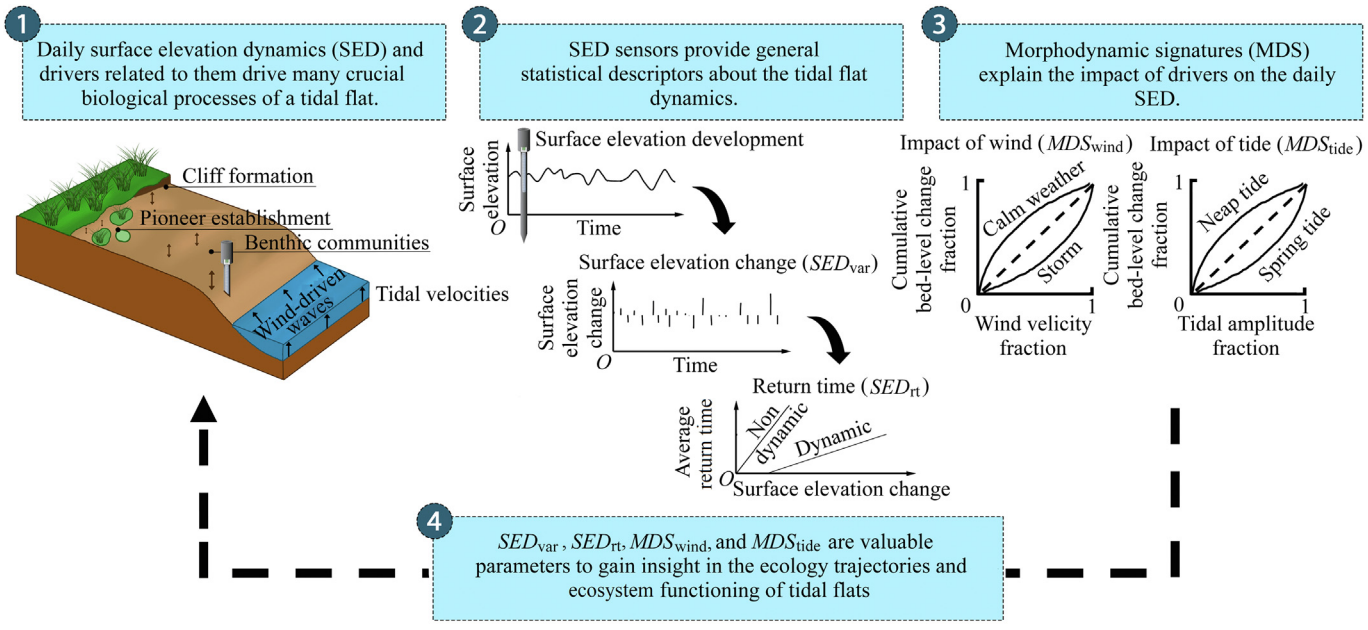

Fig. 1. Conceptual visualization of (1) relevance of studying daily surface elevation changes, (2) how statistical indices of surface elevation change over time, (3) how these indices relate to environmental drivers, and (4) how these drivers provide new knowledge about tidal flat ecosystems.

variations in wind speed (MDS_{wind}) and tidal amplitude (MDS_{tide}). This approach for deriving these empirical relationships was applied to two areas with large-scale human interventions. The aim was to create a less dynamic tidal flat habitat that would accrete over time. SED sensors were deployed at these two sites for five years. At the end of this article, we discussed how the SED and MDS signatures could be used in the future to study the ecosystem functioning of tidal flats.

2. Methods

2.1. Study sites

The MDS of the SED concept was tested at two study sites located in the Western Scheldt, an estuary in the southwestern region of the Netherlands (Fig. 2). In 2005, the Dutch and Belgian governments signed the "Ontwikkelingsschets 2010 Schelde-estuarium" convention to implement several projects to develop a sustainable Scheldt estuary with a balance between safety, accessibility, and nature. At the fringes of the tidal flats, Baalhoek (51°22′N, 4°4′E) and Knuitershoek (51°23′N, 3°58′E), existing groynes were heightened (the dashed red line in Fig. 2) or new ones were created (the solid red line in Fig. 2) to reduce hydrodynamic forces. The goals of reducing these forces were (1) to enhance sediment accretion on top of a hard peat bank and (2) to create a less dynamic habitat that increases the abundance of benthic invertebrates. The blue points on the map (Fig. 2) indicate the locations of the deployed SED sensors that were sometimes combined with wave loggers (the yellow points in Fig. 2). At all locations, elevation was regularly measured with a differential geographic information system (dGPS) (Fig. 2).

After the construction of the groynes in 2016, sedimentation was observed near the locations of all groynes (Fig. 3). The elevation change for the center treatment of Baalhoek was

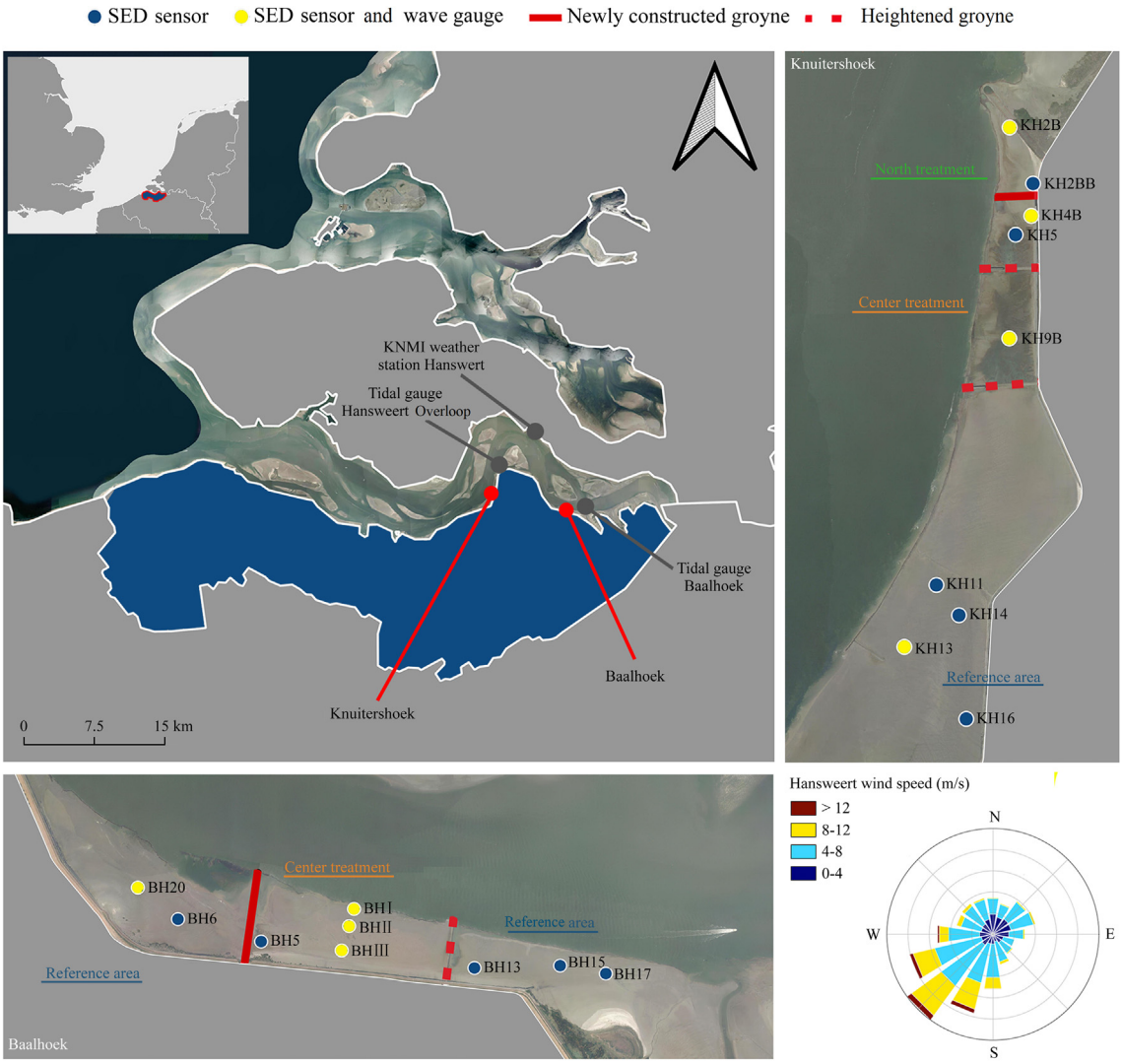

Fig. 2. Location and overview of Baalhoek and Knuitershoek in the Western Scheldt estuary, located at the northern part of Zeeuws-Vlaanderen (blue area), the Netherlands (with aerial picture from ESRI imagery 2021).

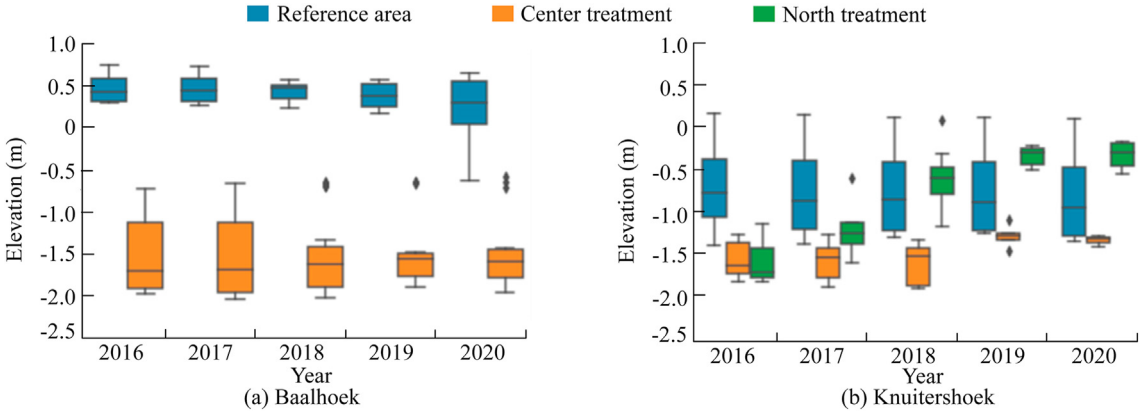

Fig. 3. Boxplots showing average annual elevation measured with a dGPS at each SED sensor location near Baalhoek and Knuitershoek (dGPS measurements with different treatments were combined).

less apparent compared to Knuitershoek, but the spatial variation in surface elevation became smaller over time, and the flattening of the tidal flat was observed (Fig. 3). The reference areas were dominated by fine sand with a median grain size (D_{50}) of 103 μm. At Baalhoek, the grain size within the groynes was similar to that of the reference area. At Knuitershoek, the area between the two northern groynes appeared less cohesive (D_{50} = 155 μm) than the locations between other groynes (D_{50} = 29 μm).

Daily wind data (2016−2021) were retrieved from the nearby Hansweert Royal Netherlands Meteorological Institute (KNMI) weather station (Fig. 2). The prevailing wind direction was southwest, with a mean wind speed of 5.7 m/s. In general, the groynes provided shelters for storm waves by dampening the height of significant waves, but they did not affect the conditions of typical waves (Appendix A). Baalhoek is sheltered from the prevailing wind direction, but the groynes of Baalhoek are perpendicular to common northwestern storms, which results in more substantial wave dampening for higher waves compared to Knuitershoek. According to a numerical model, significant changes occurred after the construction of the groynes when the current decreased from an initial range of 0.6−1.0 m/s to a value of 0.1 m/s (van Dam et al., 2008). Rijkswaterstaat provided tidal gauge measurements for the stations Baalhoek and Hansweert Overloop (Fig. 2). At Baalhoek, the average tidal amplitude was 5.0 m, with a minimum amplitude of 2.1 m and a maximum of 6.7 m. Knuitershoek had an average tidal amplitude of 4.6 m, a minimum of 1.5 m, and a maximum of 6.3 m. The construction of the groynes did not influence the tidal regime.

2.2. Monitoring daily SED after construction of groynes

After the construction of the groynes, 18 optical SED sensors were deployed between June 2016 and April 2021 to measure the SED of the intertidal flat with a high vertical and temporal resolution (Hu et al., 2015a; Willemsen et al., 2018) (Fig. 2 and Appendix B). The function of the optical SED sensor is based upon the presence of light. Essentially, 200 light-sensitive cells measure the light intensity over a 400-mm domain, resulting in an accuracy of 2−4 mm (Hu et al., 2015a; Willemsen et al., 2018). The transition from cells that receive daylight to cells that do not represent the position of the bed level. As the sensor relies on daylight, it can only perform measurements during low tides and daytime. To obtain enough data, the measurement interval was set to take one measurement every 30 min. The surface next to the SED sensors was measured every quarter year to half year with a dGPS, which was used to correct the time series measurements after replacing a SED sensor for maintenance. Raw data from the SED sensors were converted and automatically corrected for scouring or biofouling according to the method developed by Willemsen et al. (2018). The detected surface elevations were coarse-grained by calculating the observed median surface elevation of a day to enable the correlation of multiple datasets at later stages of this study (e.g., wind and tidal amplitude datasets).

2.3. General statistical indices of surface elevation

First, general statistical indices of the surface elevation were calculated to examine the surface elevation trajectory of the tidal flat based on the time series measured by the SED sensors: (1) average surface elevation, (2) surface elevation variance, and (3) surface elevation correlation length (Appendix C). Locations with relatively stable bed levels have low surface elevation variances, whereas those with more fluctuations in surface elevation have higher variances. The autocorrelation function (ACF) indicates the persistence of surface elevation over the total measurement length in days (n). To derive the ACF, temporal autocorrelation was calculated by stepwise increasing the lags of daily measurements up to half of the total measurement period (n/2):

$$F_{\mathrm{AC}}\left(t_{\mathrm{lag}}\right) = R\left(z_i, z_{i+t_{\mathrm{lag}}}\right) \tag{1}$$

where F_{AC} is the ACF; t_{lag} is the lag time (d); R is the temporal autocorrelation function; z_i is the surface elevation at time i; and $z_{i+t_{lag}}$ is the surface elevation at time $i + t_{lag}$. The correlation length (in days) was defined as the lag time at which $F_{AC} \leq 1/e$ where e is the natural constant. The correlation length is an essential proxy representing how quickly conditions change for organisms that need to cope with environmental fluctuations. If the correlation length increases over time (longer than t_{lag}), the location becomes more suitable for organisms because vegetation or benthic invertebrates need a period with stable environmental conditions to tolerate disturbances (van Belzen et al., 2022). To indicate whether a trend existed in the surface elevation, the Kendall's tau test was performed. This test measured the correlation between the variable time and surface elevation, in which time was a ranked factor.

2.4. SED indices

For many biophysical processes, it is important to understand the position and trend of the surface elevation, and it is even more important to study the daily SED (Figs. 1 and 2). In particular, the changes in timing and magnitude relate to the establishment and recruitment of species (van Belzen et al., 2022). Therefore, the difference vector for the daily surface elevation changes over time (δ) was obtained. To avoid significant outliers in the surface elevation change, outliers caused by measurement errors related to the disturbance of the light-sensitive cells of the sensors, the values in the lower and upper 1% of the δ dataset were removed. Given δ was known, the variance of the daily surface elevation change (var $\boldsymbol{\delta}$) can be analyzed. The variance is another indicator to express the probability of ecosystem emergence (van Belzen et al., 2022).

To relate physical processes to the surface elevation changes, a division was made between accretion and erosion. Both of these processes occur under different circumstances. First, a dataset of negative surface elevation changes ($\boldsymbol{\delta}_{ero}$) was compiled:

$$\delta_{i,ero} = |z_{i+1} - z_i| \quad z_{i+1} < z_i \tag{2}$$

where $\delta_{i,ero}$ is the negative surface elevation change at time i, and z_{i+1} is the surface elevation at time $i + 1$. The dataset of positive surface elevation changes ($\boldsymbol{\delta}_{acc}$) was derived on the condition of $z_i < z_{i+1}$.

2.4.1. SED average variability (SED_{var})

Based on the $\boldsymbol{\delta}_{ero}$ or $\boldsymbol{\delta}_{acc}$ datasets, the SED average variability (SED_{var}) was derived. SED_{var} is the sum of $\boldsymbol{\delta}_{ero}$ or $\boldsymbol{\delta}_{acc}$ divided by the total measurement length in days (n). This is a quantitative description of the average magnitude of the surface elevation change per day, an index that is rarely quantified in terms of space and time.

2.4.2. SED return time (SED_{rt})

The return time indicates how often the surface elevation change with a certain magnitude may occur. It expresses the possibility that a daily SED exceeds the threshold for establishment. Like SED_{var}, erosion and accretion events were considered separately. To retrieve the return time for all observed bed level changes (T_r), all elements in δ_{acc} and δ_{ero} were ranked in descending order, and serial numbers from 1 to n were given. The frequency of exceedance (F) denoting an event that does not exceed the ranked bed level change was calculated as

$$F(\delta_i < \delta_r) = \frac{r}{l+1} \tag{3}$$

where δ_i is the bed level change on the ith day, δ_r is the daily bed level change with a rank of r in descending order, and l is the total number of days with observed bed level changes for erosion or accretion. T_r can therefore be derived as

$$T_r(\delta_i) = \frac{1}{F(\delta_i < \delta_r)} \tag{4}$$

It was assumed that the extensive time series were representative for SED. This assumption made it possible to derive the quantitative descriptions for the return time over more extensive periods. These descriptions could be used to predict the return time of larger events that did not occur during the measurement period. One quantitative description for the return time, the SED return index (SED_{rt}), can be derived as

$$T_r(\delta_i) = SED_{rt}^{F(\delta_i < \delta_r)} \tag{5}$$

The SED_{rt} index is particularly relevant to assessment of the impact of the short-term dynamics on the long-term evolution of the tidal flat. Larger values of this index represent less dynamic locations, and smaller values represent more dynamic locations.

2.5. MDS indices

The aforementioned statistical indices aimed to characterize SED, but they did not consider the relation to environmental drivers that cause surface elevation variability. In this section, an analytical method was developed to determine the relative contribution of environmental drivers to short-term surface elevation changes by pairing daily SED with publicly available time series of wind and tidal amplitudes (Figs. 1 through 3). The MDS analysis considers which environmental conditions, $\boldsymbol{\delta}_{acc}$ or $\boldsymbol{\delta}_{ero}$, are more likely to occur. It thereby quantifies the sensitivity of the driver to variations. This section presents two MDSs characterizing the impacts of wind speed as an indicator for wind-driven waves and tidal amplitude as an indicator for the maximum current velocity (Bouma et al., 2005).

2.5.1. Morphodynamic wind signature (MDS_{wind})

First, daily measurements of $\boldsymbol{\delta}_{acc}$ or $\boldsymbol{\delta}_{ero}$ were paired with publicly available daily wind speed (U) time series retrieved from the nearest KNMI weather station (Fig. 2). Subsequently, the resulting time series were sorted according to ascending U.

Fifty evenly spaced intervals (I) between zero and the maximum observed wind speed (U_{max}) were defined. Then, the number of days (M) with a given U exceeding an interval was calculated and normalized by the total number of days in the dataset (l). This process yielded the fraction f_{wind}:

$$f_{wind} = \frac{M}{l} \tag{6}$$

$f_{wind} = 0$ represents the lowest observed wind speed, $f_{wind} = 1$ represents the maximum wind speed, and $f_{wind} = 0.5$ represents the median wind speed. For each wind fraction, the sum of $\boldsymbol{\delta}_{acc}$ or $\boldsymbol{\delta}_{ero}$ for all daily wind speeds up to that fraction was calculated and normalized by the sum of accretion or erosion, respectively. This process yielded the surface elevation change fraction (f_δ) as a function of I:

$$f_\delta = \sum_{0 \le U \le I} \delta_i \Big/ \sum_{i=1}^{N} \delta_i \tag{7}$$

where δ_i is the ith positive or negative surface elevation change, and N is the total number of days with positive or negative surface elevation changes. The relation between f_{wind} and f_δ can take different shapes depending on the sensitivity of the tidal flat morphodynamics to either stormy or calm conditions. This relation was characterized by a power law equation (Appendix D), yielding the constant MDS_{wind}:

$$f_\delta = f_{wind}^{MDS_{wind}} \tag{8}$$

This functional equation was derived from the data presented in this study. The coefficients of determination (R^2) for all 18 locations indicated that the equation fitted well ($R^2 > 0.93$). An MDS_{wind} value near 1 indicates that the patterns of surface elevation variation are uncorrelated with the changes in wind speed (Appendix D). Values less than 1 denote surface elevation changes dominated by calm weather conditions. Meanwhile, surface elevations at locations with MDS_{wind} values higher than 1 are dominated by storm conditions. R^2 was calculated for the power−law equation. If an unsatisfied fit was acquired, the correlation could be improved by changing the interval size.

2.5.2. Morphodynamic tide signature (MDS_{tide})

MDS_{tide} was retrieved similarly to the constant MDS_{wind}, but wind data were replaced with the maximum tidal range per day, as measured at the publicly available Rijkswaterstaat tidal gauge stations (Fig. 2). MDS_{tide} expresses the magnitude of the morphodynamic tide force (Appendix D). MDS_{tide} values less than 1 denote surface elevation changes dominated by neap-tide periods, while values high than 1 indicate that surface elevation changes are dominated by spring-tide periods.

2.6. Statistical tests

For the case study, we assessed whether the construction of groynes had a significant impact on the indices. One-way analysis of variance (ANOVA) was performed to compare the effect of groyne construction on each index. The test was performed over the reference and treatment groups.

3. Results

Independent from the position related to the groynes, a significant trend of surface elevation was observed at all locations during the five-year measurement period (Appendix E). The surface elevation of the reference areas declined over time (−0.11 mm/d). The center treatments accreted slightly (0.03 mm/d), and the north treatment experienced a strong accretion (1.16 mm/d) (Appendix E). This accretion was related to the change in the tidal current velocity from 1.0 m/s to 0.1 m/s, which was observed at all locations. Furthermore, the surface elevation variance increased in the areas close to the groynes ($p < 0.01$), indicating that the tidal flats moved away from the more stable state of the reference areas (low variance). No correlation length was observed for the northern treatment. Compared to the reference areas, the correlation length for the center treatments (102 d) was significantly longer (34 d, $p < 0.05$; Appendix E). Thus, longer correlation lengths favored the ecological processes.

3.1. SED average variability (SED_{var})

In the reference areas, SED_{var} was observed to have high rates of accretion and erosion at Baalhoek ((4.7 ± 0.5) mm/d and (−4.7 ± 0.3) mm/d, respectively) and Knuitershoek ((4.8 ± 1.2) mm/d and (−5.0 ± 1.2) mm/d, respectively) (Figs. 4(a), 5(a), and 6(c) and (d)). SED_{var} for the areas sheltered by the groynes was 1−2 orders of magnitude smaller than the reference areas for the center treatment of both Baalhoek ((3.7 ± 0.6) mm/d and (−3.5 ± 0.6) mm/d for accretion and erosion, respectively) and Knuitershoek ((1.9 ± 0.1) mm/d and (−2.1 ± 0.1) mm/d for accretion and erosion, respectively). Compared to the center treatment, the north treatment of Knuitershoek was exposed to slightly stronger accretion and erosion dynamics ((4.9 ± 0.1) mm/d and (−3.6 ± 0.2) mm/d, respectively). Between the reference and treatments, a significant difference was observed in the accretion and erosion rates at Baalhoek ($p < 0.05$ and $p < 0.01$, respectively) and Knuitershoek ($p < 0.01$ and $p < 0.05$, respectively). These results reflected that the magnitude of daily SED near the groynes was reduced compared to the reference areas. This reduction was caused by the reduction in hydrodynamics (e.g., wave extremes and tidal currents) and by the change in sediment characteristics (more cohesive).

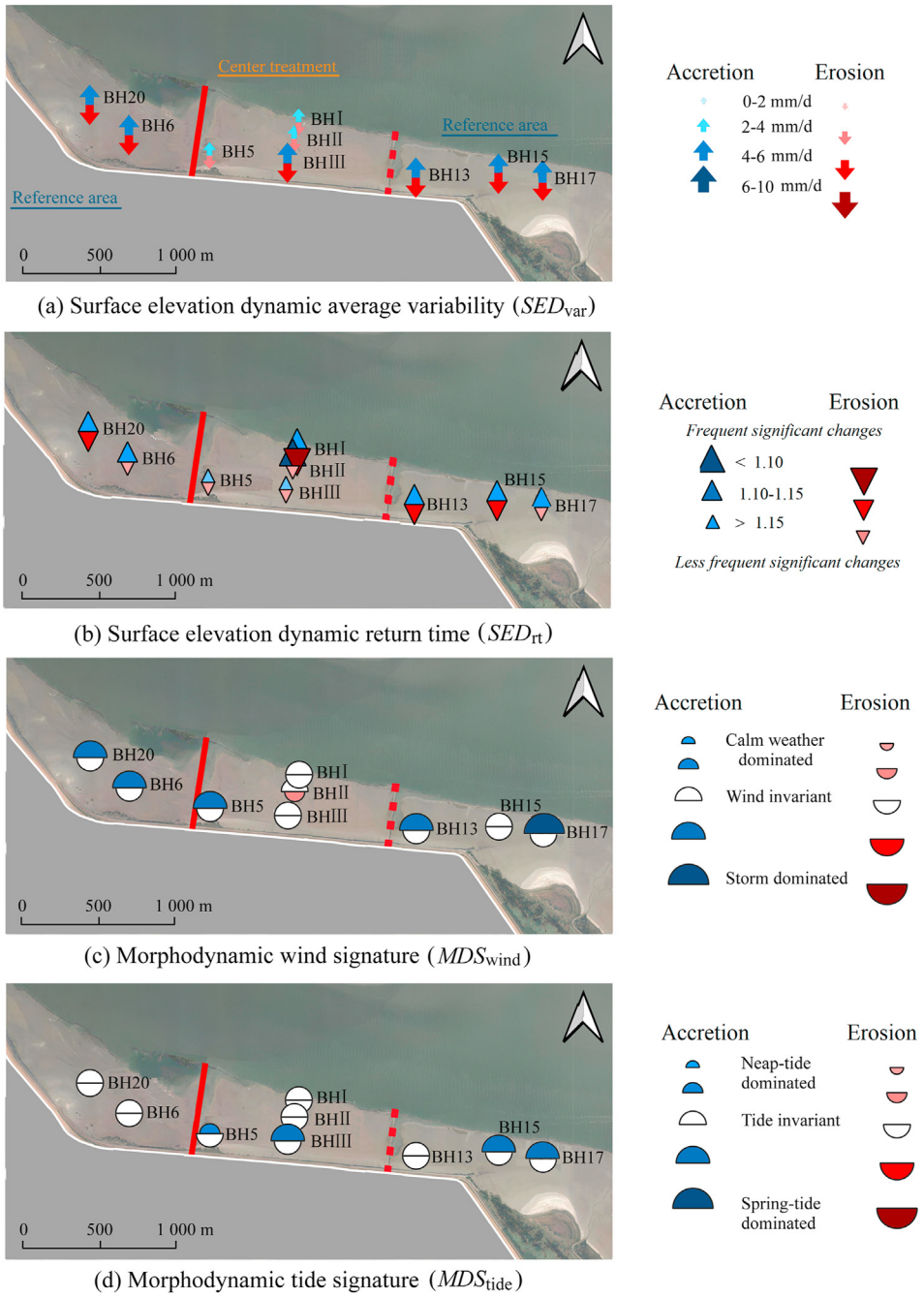

(a) Surface elevation dynamic average variability (SED_{var})

(b) Surface elevation dynamic return time (SED_{rt})

(c) Morphodynamic wind signature (MDS_{wind})

(d) Morphodynamic tide signature (MDS_{tide})

Fig. 4. Derivation of four major statistical indices for surface elevation change at Baalhoek (large and dark symbols indicate significant accretion or erosion fluxes/signatures, and small and light symbols indicate less impacted trends during calm periods of wind or tide).

3.2. SED return time (SED_{rt})

The center treatment of Knuitershoek had a short return time of significant surface elevation changes for both accretion and erosion (1.37 ± 0.06 and 1.35 ± 0.02, respectively). Changes with certain magnitudes occurred at the same interval, indicating a relatively stable bed level elevation. In contrast, the reference area exhibited a difference in magnitude for the sedimentation and erosion return times (1.35 ± 0.02 and 1.13 ± 0.07, respectively) (Figs. 4(b), 5(b), and 6(e) and (f)). The northern treatment of Knuitershoek, however, showed similar long return times for both accretion and erosion (1.13 ± 0.03 and 1.17 ± 0.05, respectively). At Knuitershoek, the return times for accretion and erosion differed significantly between the three locations ($p < 0.05$ and $p < 0.01$, respectively). At Baalhoek, no significant difference was observed between the accretion and erosion return times at the center treatment (1.12 ± 0.05 and 1.15 ± 0.03, respectively) and reference area (1.15 ± 0.01 and 1.16 ± 0.02, respectively).

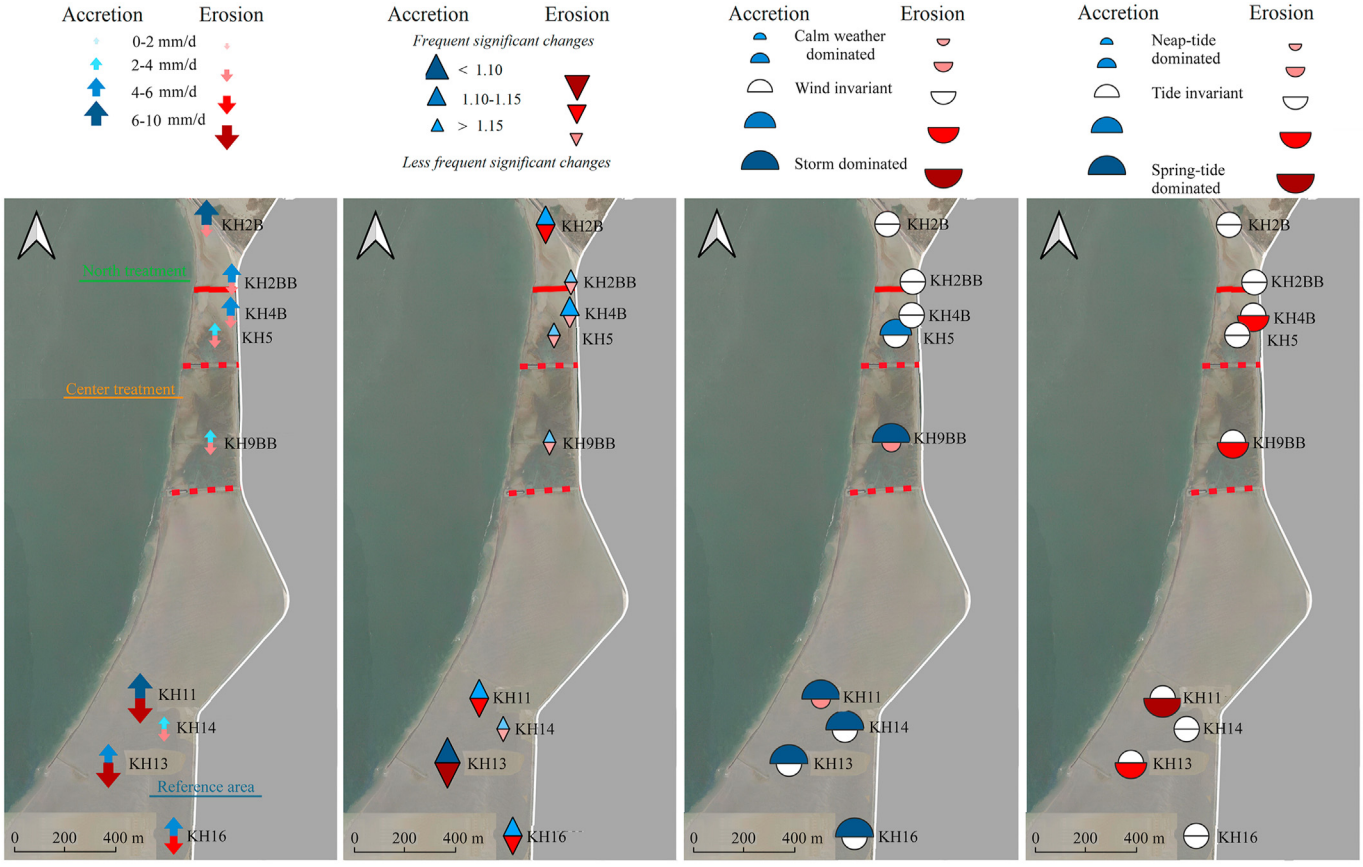

(a) Surface elevation dynamic average variability (SED_{var})

(b) Surface elevation dynamic return time (SED_{rt})

(c) Morphodynamic wind signature (MDS_{wind})

(d) Morphodynamic tide signature (MDS_{tide})

Fig. 5. Derivation of four major statistical indices for surface elevation change at Knuitershoek (large and dark symbols indicate significant accretion or erosion fluxes/signatures, and small and light symbols indicate less impacted trends during calm periods of wind or tide).

3.3. Morphodynamic wind signature (MDS_{wind})

The MDS_{wind} values of almost all reference areas indicated that the surface elevation was dominated by sedimentation during high wind speed periods (1.63 ± 0.44). This pattern could most likely be explained by the redistribution of eroded sediments from other parts of the estuary. The erosion processes in the reference areas were independent of the prevailing wind conditions in both reference and treatment areas (0.93 ± 0.11) (Figs. 4(c), 5(c), and 6(g) and (h)). Nonetheless, the influence of wind on accretion decreased gradually around the groynes until wind became invariant (1.11 ± 0.15). This indicated that, compared to the reference areas, sedimentation dynamics near the groynes were significantly less influenced by the wind force ($p < 0.05$). The reduction toward wind invariance could be explained by the observed reduction in peak wave height near the constructed groynes (Appendix A). The most significant dampening occurred near the Baalhoek groynes that are almost perpendicular to the wind during northwest storms. This site is sheltered from southwest storms. Since the groynes provide shelter for the wind fetch, SED became invariant of wind conditions, as presented by MDS_{wind}. Compared to the reference areas, no significant impact was observed for the erosion dynamics near the groynes. No correlation existed between sediment dynamics and wind direction at these intervention sites.

3.4. Morphodynamic tide signature (MDS_{tide})

Some sites showed a minor influence of spring tides on the sediment dynamics. Nevertheless, the influence of tides was demonstrated to be invariant in most locations for both erosion (1.11 ± 0.14) and sedimentation dynamics (1.02 ± 0.13) (Figs. 4(d), 5(d), and 6(i) and (j)). No statistical evidence was found that the groynes significantly changed the influence of tides on short-term erosion or sedimentation.

4. Discussion and conclusions

4.1. Effect of groynes on tidal flat trajectory

The statistical descriptors and indices provide a spatially explicit understanding of sediment dynamics that drive ecosystem dynamics, an understanding that surpasses the common hydrodynamic characterization of tidal flats (Appendix E). Up to a certain level, however, hydrodynamics

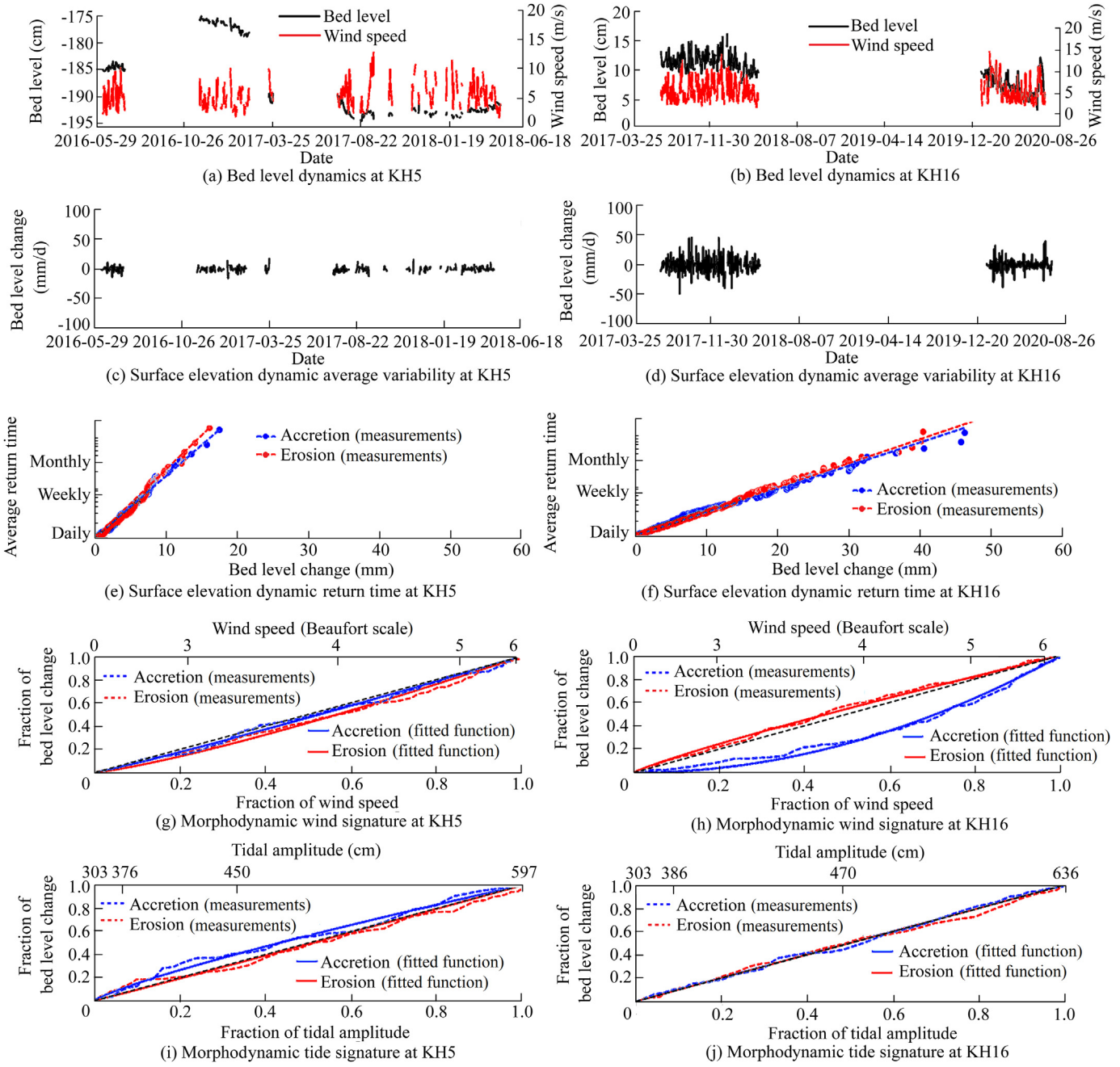

Fig. 6. An example of SED and MDS analyses for center treatment KH5 and reference area SED sensors KH16. The surface elevation ((a) and (b)) showed a higher magnitude of SED_{var} for KH16 ((c) and (d)), which had a higher return period compared to the treatment locations ((e) and (f)). The reference area experienced wind dominated accretion, while wind had no impact on the treatment locations ((g) and (h)). All locations were invariant for events in the tidal cycle ((i) and (j)).

can be characterized within the presented statistical generalization of MDS. This study did not aim to explain the impacts of hydrodynamics and sediment characteristics on sediment dynamics. Instead, it quantified the sediment dynamics that drive seedling establishment or benthos settlement. In general, the presented results of the empirical statistical indices revealed that the construction of groynes affects the morphodynamics of a tidal flat. The observed reductions in both the amplitude (SED_{var}) and period (SED_{rt}) of surface elevation change potentially favor benthos settlement (Bouma et al., 2001; Nambu et al., 2012; van Belzen et al., 2022). In agreement with previous studies, we found the evidence for the absence of tidal impact on the short-term SED. Hence, wind-generated waves are the main drivers of disturbances on the surface elevation of tidal flats (Green et al., 1997; Christie et al., 1999; Callaghan et al., 2010; Zhu et al., 2014; de Vet et al., 2020). These results are consistent with previously modelled results and with the goal of the intervention to devise, on average, smaller daily

surface elevation dynamics and create a sheltered and accreting tidal flat (van Dam et al., 2008).

4.2. Added value of statistical indices for understanding of SED

Sedimentation and erosion processes on tidal flats often relate to the impacts of wind-driven waves or storm conditions (Kohsiek et al., 1988; Zhu et al., 2017; de Vet et al., 2020). Seasonal-scale variations in sediment stability occur due to the presence of biofilms (Paarlberg et al., 2005) or bioturbation (Bouma et al., 2001; Nambu et al., 2012). Most of the time, these biophysical event–driven processes are difficult to capture in process-based morphodynamic models or in conventional field campaigns (e.g., acoustic doppler velocimetry (ADV), acoustic doppler current profiler (ADCP), and light detection and ranging (LiDAR)), which are regularly limited in temporal or spatial resolutions. The annual and daily time series of bed level dynamics measured by SED sensors are complementary to understanding and prediction of tidal flat evolution and resilience (Hu et al., 2015a, 2017). The general statistical indices presented in this study provide valuable insights into both the daily and annual morphodynamic development of tidal flats. In more depth, the SED indices analyze the magnitude (SED_{var}) and timing (SED_{rt}) of SED, which can serve as indicators for understanding of the role of physical processes on the establishment of pioneer vegetation (Balke et al., 2011; Bouma et al., 2016; Cao et al., 2018), the settlement of benthic invertebrates (Bouma et al., 2001, 2016; Nambu et al., 2012; Shi et al., 2021), and the dislodgement caused by surface elevation changes during storms (de Vet et al., 2020). The MDS indices present the role of disturbance events on the sediment dynamics and trajectory of tidal flats. The MDS_{wind} results provide evidence of whether wind-driven waves affect the daily surface elevation change (Fagherazzi et al., 2007; Belliard et al., 2019; de Vet et al., 2020). Prior work has noted the importance of low elevated tidal flat trajectories to tides (Belliard et al., 2019). The impact of the tidal cycle can be analyzed with MDS_{tide}. Hence, the statistical indices (Appendix C) facilitate an innovative method to study the morphodynamics of high to low dynamic tidal flats across different timescales.

4.3. Limitations of statistical indices

The findings may be somewhat limited by the spatial resolution or temporal coverage of the SED datasets. The statistical indices presented here only indicate the trends observed at a specific location, but tidal flat systems can be heterogenous over short distances. Furthermore, the indices do not explicitly capture extreme events with return times exceeding the measurement duration. Nonetheless, SED_{rt} that allows for extrapolation comparable to extreme water level predictions are based on extrapolations of the return time (Kirezci et al., 2020). Due to the increasing critical bed shear stress with depth (Zhu et al., 2016) and local sediment availability (Li et al., 2014), these indices cannot account for physical limits in erosion or sedimentation.

The MDS concept implies that variations in other conditions cannot explain the observational statistics for a specific location. In other words, it is loosely suggested that other natural forces remain irrelevant over extended measurement periods for the specific location (Friedrichs, 2011). Other viable MDS indices could explain other morphodynamic processes, such as variations in river discharge (Yang et al., 2008), suspended sediment concentrations (Li et al., 2014), and the variability in bioturbator abundance and species composition (Cozzoli et al., 2018; de Smit et al., 2022).

4.4. Outlook: implications for understanding of habitat suitability and climate change sensitivity of tidal flats

The SED and MDS analyses provide a simplified approach that governs our understanding of the morphodynamic evolution of intertidal flats based on the medium-term SED. Future studies can use these indices as a tool to gain more knowledge about the functioning of tidal flat ecosystems (Figs. 1 through 4). For example, if we understand how sediment dynamics affect species communities and settlement, this understanding might enable us to predict the responses to large-scale interventions (Fig. 7). Significant magnitudes and return times of surface elevation change can affect the success of establishment for vegetation or benthic communities, while limited magnitudes and return times favor the establishment. Furthermore, by applying a statistical generalization over the observed patterns, MDS can support the work designed to better understand the sensitivity of tidal flats to climate change or sea level rise (i.e., de Smit et al., 2021). These findings may be somewhat limited because they focus on the magnitude rather than the specific timing of the forcing process (de Vet et al., 2020). It is, however, impossible to predict the timing of specific events. Hence, statistical generalizations remain a powerful tool for sensitivity analyses. In conclusion, SED and MDS analyses are promising tools of statistical observation and can provide valuable information on the short-term surface elevation dynamics. In context, they can help researchers

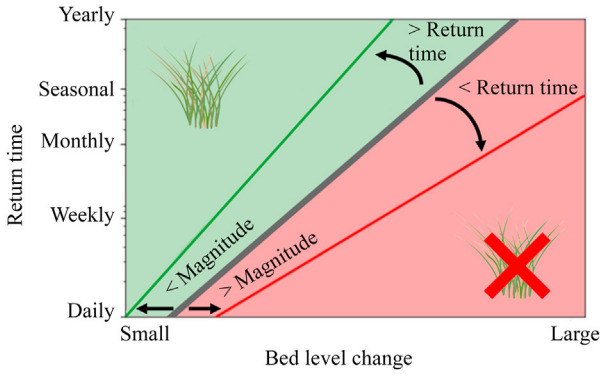

Fig. 7. Species most likely have a threshold in magnitude (horizontal axis) and period (vertical axis) for their establishment (grey line).

understand and predict ecosystem trajectories under changing conditions, such as human measures (e.g., construction of dams and coastal constructions) and climate change.

Declaration of competing interest

The authors declare no conflicts of interest.

Appendices A−E. Supplementary data

Supplementary data to this article can be found online at https://doi.org/10.1016/j.wse.2022.11.003.

References

Balke, T., Bouma, T.J., Horstman, E.M., Webb, E.L., Erftemeijer, P.L., Herman, P.M., 2011. Windows of opportunity: Thresholds to mangrove seedling establishment on tidal flats. Mar. Ecol. Prog. Ser. 440, 1−9. https://doi.org/10.3354/meps09364.

Barbier, E.B., 2019. Chapter 27 - The value of coastal wetland ecosystem services. In: Perillo, G.M.E., Wolanski, E., Cahoon, D.R., Hopkinson, C.S. (Eds.), Coastal Wetlands, An Integrated and Ecosystem Approach, Second Edition. Elsevier, Amsterdam, pp. 947−964.

Belliard, J.P., Silinski, A., Meire, D., Kolokythas, G., Levy, Y., Van Braeckel, A., Bouma, T.J., Temmerman, S., 2019. High-resolution bed-level changes in relation to tidal and wave forcing on a narrow fringing macrotidal flat: Bridging intra-tidal, daily and seasonal sediment dynamics. Mar. Geol. 412, 123−138. https://doi.org/10.1016/j.margeo.2019.03.001.

Bouma, H., Duiker, J., De Vries, P., Herman, P., Wolff, W., 2001. Spatial pattern of early recruitment of *Macoma balthica* (L.) and *Cerastoderma edule* (L.) in relation to sediment dynamics on a highly dynamic intertidal sandflat. J. Sea Res. 45(2), 79−93. https://doi.org/10.1016/S1385-1101(01)00054-5.

Bouma, T.J., De Vries, M.B., Low, E., Kusters, L., Herman, P.M.J., Tanczos, I.C., Temmerman, S., Hesselink, A., Meire, P., Regenmortel, S.V., 2005. Flow hydrodynamics on a mudflat and in salt marsh vegetation: Identifying general relationships for habitat characterisations. Hydrobiologia 540(1), 259−274. https://doi.org/10.1007/s10750-004-7149-0.

Bouma, T.J., van Belzen, J., Balke, T., van Dalen, J., Klaassen, P., Hartog, A., Callaghan, D., Hu, Z., Stive, M., Temmerman, S., et al., 2016. Short-term mudflat dynamics drive long-term cyclic salt marsh dynamics. Limnol. Oceanogr. 61(6), 2261−2275. https://doi.org/10.1002/lno.10374.

Callaghan, D.P., Bouma, T.J., Klaassen, P., van der Wal, D., Stive, M.J.F., Herman, P.M.J., 2010. Hydrodynamic forcing on salt-marsh development: Distinguishing the relative importance of waves and tidal flows. Estuar. Coast. Shelf Sci. 89(1), 73−88. https://doi.org/10.1016/j.ecss.2010.05.013.

Cao, H., Zhu, Z., Balke, T., Zhang, L., Bouma, T.J., 2018. Effects of sediment disturbance regimes on *Spartina* seedling establishment: Implications for salt marsh creation and restoration. Limnol. Oceanogr. 63(2), 647−659. https://doi.org/10.1002/lno.10657.

Christie, M., Dyer, K., Turner, P., 1999. Sediment flux and bed-level measurements from a macro tidal mudflat. Estuar. Coast. Shelf Sci. 49(5), 667−688. https://doi.org/10.1006/ecss.1999.0525.

Cozzoli, F., Bouma, T.J., Ottolander, P., Lluch, M.S., Ysebaert, T., Herman, P.M., 2018. The combined influence of body size and density on cohesive sediment resuspension by bioturbators. Sci. Rep. 8(1), 1−12. https://doi.org/10.1038/s41598-018-22190-3.

de Smit, J.C., Brückner, M.Z., Mesdag, K.I., Kleinhans, M.G., Bouma, T.J., 2021. Key bioturbator species within benthic communities determine sediment resuspension thresholds. Front. Mar. Sci. 8, 726238. https://doi.org/10.3389/fmars.2021.726238.

de Smit, J.C., Bin Mohd Noor, M.S., Infantes, E., Bouma, T.J., 2022. Wind exposure and sediment type determine the resilience and response of seagrass meadows to climate change. Limnol. Oceanogr. 67, S121−S123. https://doi.org/10.1002/lno.11865.

de Vet, P.L.M., van Prooijen, B.C., Wang, Z.B., 2017. The differences in morphological development between the intertidal flats of the Eastern and Western Scheldt. Geomorphology 281, 31−42. https://doi.org/10.1016/j.geomorph.2016.12.031.

de Vet, P.L.M., van Prooijen, B.C., Schrijvershof, R.A., van der Werf, J.J., Ysebaert, T., Schrijver, M.C., Wang, Z.B., 2018. The importance of combined tidal and meteorological forces for the flow and sediment transport on intertidal shoals. J. Geophys. Res.: Earth Surf. 123(10), 2464−2480. https://doi.org/10.1029/2018JF004605.

de Vet, P.L.M., van Prooijen, B.C., Colosimo, I., Steiner, N., Ysebaert, T., Herman, P.M.J., Wang, Z.B., 2020. Variations in storm-induced bed-level dynamics across intertidal flats. Sci. Rep. 10, 12877. https://doi.org/10.1038/s41598-020-69444-7.

de Vriend, H.J., Wang, Z.B., Ysebaert, T., Herman, P.M., Ding, P., 2011. Eco-morphological problems in the Yangtze estuary and the Western Scheldt. Wetlands 31(6), 1033−1042. https://doi.org/10.1007/s13157-011-0239-7.

Fagherazzi, S., Palermo, C., Rulli, M.C., Carniello, L., Defina, A., 2007. Wind waves in shallow microtidal basins and the dynamic equilibrium of tidal flats. J. Geophys. Res.: Earth Surf. 112, F02024. https://doi.org/10.1029/2006JF000572.

Fagherazzi, S., Mariotti, G., Leonardi, N., Canestrelli, A., Nardin, W., Kearney, W.S., 2020. Salt marsh dynamics in a period of accelerated sea level rise. J. Geophys. Res.: Earth Surf. 125, e2019JF005200. https://doi.org/10.1029/2019JF005200.

Friedrichs, C.T., 2011. 3.06 - tidal flat morphodynamics: A synthesis. In: Wolanski, E., McLusky, M. (Eds.), Treatise on Estuarine and Coastal Science. Academic Press, Pittsburgh, pp. 137−170. https://doi.org/10.1016/B978-0-12-374711-2.00307-7.

Goldberg, L., Lagomasino, D., Thomas, N., Fatoyinbo, T., 2020. Global declines in human-driven mangrove loss. Global Change Biol. 26, 5844−5855. https://doi.org/10.1111/gcb.15275.

Green, M.O., Black, K.P., Amos, C.L., 1997. Control of estuarine sediment dynamics by interactions between currents and waves at several scales. Mar. Geol. 144(1−3), 97−116. https://doi.org/10.1016/S0025-3227(97)00065-0.

Hu, Z., Lenting, W., van der Wal, D., Bouma, T.J., 2015a. Continuous monitoring bed-level dynamics on an intertidal flat: Introducing novel, stand-alone high-resolution SED-sensors. Geomorphology 245, 223−230. https://doi.org/10.1016/j.geomorph.2015.05.027.

Hu, Z., Wang, Z.B., Zitman, T.J., Stive, M.J., Bouma, T.J., 2015b. Predicting long-term and short-term tidal flat morphodynamics using a dynamic equilibrium theory. J. Geophys. Res.: Earth Surf. 120, 1803−1823. https://doi.org/10.1002/2015JF003486.

Hu, Z., Yao, P., van der Wal, D., Bouma, T.J., 2017. Patterns and drivers of daily bed-level dynamics on two tidal flats with contrasting wave exposure. Sci. Rep. 7, 7088. https://doi.org/10.1038/s41598-017-07515-y.

Hu, Z., van der Wal, D., Cai, H., van Belzen, J., Bouma, T.J., 2018. Dynamic equilibrium behaviour observed on two contrasting tidal flats from daily monitoring of bed-level changes. Geomorphology 311, 114−126. https://doi.org/10.1016/j.geomorph.2018.03.025.

Hu, Z., Willemsen, P.W.J.M., Borsje, B.W., Wang, C., Wang, H., van der Wal, D., Zhu, Z., Oteman, B., Vuik, V., Evans, B., Möller, I., Belliard, J.P., van Braeckel, A., Temmerman, S., Bouma, T.J., 2021. Synchronized high-resolution bed-level change and biophysical data from 10 marsh-mudflat sites in northwestern Europe. Earth Syst. Sci. Data 13, 405−416. https://doi.org/10.5194/essd-13-405-2021.

Kirby, R., 2000. Practical implications of tidal flat shape. Continent. Shelf Res. 20(10−11), 1061−1077. https://doi.org/10.1016/S0278-4343(00)00012-1.

Kirezci, E., Young, I.R., Ranasinghe, R., Muis, S., Nicholls, R.J., Lincke, D., Hinkel, J., 2020. Projections of global-scale extreme sea levels and resulting episodic coastal flooding over the 21st Century. Sci. Rep. 10, 11629. https://doi.org/10.1038/s41598-020-67736-6.

Kirwan, M., Temmerman, S., 2009. Coastal marsh response to historical and future sea-level acceleration. Quat. Sci. Rev. 28(17−18), 1801−1808. https://doi.org/10.1016/j.quascirev.2009.02.022.

Kohsiek, L., Buist, H., Bloks, P., Misdorp, R., van den Berg, J., Visser, J., 1988. Sedimentary processes on a sandy shoal in a mesotidal estuary (Oosterschelde, The Netherlands). In: de Boer, P.L., van Gelder, A., Nio, S.D. (Eds.), Tide-Influenced Sedimentary Environments and Facies. Reidel, Dordrecht, pp. 201−214.

Le Hir, P., Roberts, W., Cazaillet, O., Christie, M., Bassoullet, P., Bacher, C., 2000. Characterization of intertidal flat hydrodynamics. Continent. Shelf Res. 20(12−13), 1433−1459. https://doi.org/10.1016/S0278-4343(00)00031-5.

Li, X., Zhou, Y., Zhang, L., Kuang, R., 2014. Shoreline change of Chongming Dongtan and response to river sediment load: A remote sensing assessment. J. Hydrol. 511, 432−442. https://doi.org/10.1016/j.jhydrol.2014.02.013.

Millennium Ecosystem Assessment, 2005. Ecosystems and Human Well-Being: Current State and Trends, Volume 5. Island Press, Washington DC.

Murray, N.J., Phinn, S.R., DeWitt, M., Ferrari, R., Johnston, R., Lyons, M.B., Clinton, N., Thau, D., Fuller, R.A., 2019. The global distribution and trajectory of tidal flats. Nature 565, 222−225. https://doi.org/10.1038/s41586-018-0805-8.

Nambu, R., Saito, H., Tanaka, Y., Higano, J., Kuwahara, H., 2012. Wave actions and topography determine the small-scale spatial distribution of newly settled Asari clams *Ruditapes philippinarum* on a tidal flat. Estuar. Coast. Shelf Sci. 99, 1−9. https://doi.org/10.1016/j.ecss.2011.11.010.

Paarlberg, A.J., Knaapen, M.A., de Vries, M.B., Hulscher, S.J., Wang, Z., 2005. Biological influences on morphology and bed composition of an intertidal flat. Estuar. Coast. Shelf Sci. 64(4), 577−590. https://doi.org/10.1016/j.ecss.2005.04.008.

Passeri, D.L., Hagen, S.C., Medeiros, S.C., Bilskie, M.V., Alizad, K., Wang, D., 2015. The dynamic effects of sea level rise on low-gradient coastal landscapes: A review. Earth's Future 3(6), 159−181. https://doi.org/10.1002/2015EF000298.

Saintilan, N., Khan, N.S., Ashe, E., Kelleway, J.J., Rogers, K., Woodroffe, C.D., Horton, B.P., 2020. Thresholds of mangrove survival under rapid sea level rise. Science 368(6495), 1118−1121. https://doi.org/10.1126/science.aba2656.

Shepard, C.C., Crain, C.M., Beck, M.W., 2011. The protective role of coastal marshes: A systematic review and meta-analysis. PLoS One 6(11), e27374. https://doi.org/10.1371/journal.pone.0027374.

Shi, B., Yang, S.L., Temmerman, S., Bouma, T., Ysebaert, T., Wang, S., Zhang, Y., Wu, J., Yang, H., Zhang, L., et al., 2021. Effect of typhoon-induced intertidal-flat erosion on dominant macrobenthic species (*Meretrix meretrix*). Limnol. Oceanogr. 66(12), 4197−4209. https://doi.org/10.1002/lno.11953.

Temmerman, S., Meire, P., Bouma, T., Herman, P., Ysebaert, T., De Vriend, H.J., 2013. Ecosystem-based coastal defence in the face of global change. Nature 504, 79−83. https://doi.org/10.1038/nature12859.

van Belzen, J., Fivash, G.S., Hu, Z., Bouma, T.J., Herman, P.M.J., 2022. A probabilistic framework for windows of opportunity: The role of temporal variability in critical transitions. J. R. Soc. Interface 19(190), 20220041. https://doi.org/10.1098/rsif.2022.0041.

van Dam, G., Koks, L., van Stichelen, K., 2008. Buitendijks Natuurherstel in de Westerschelde Verkenning naar Mogelijke Gebieden en Maatregelen (Report No. GD/08187/1480/C). Provincie Zeeland.

van der Wegen, M., Jaffe, B.E., 2014. Processes governing decadal-scale depositional narrowing of the major tidal channel in San Pablo Bay, California, USA. J. Geophys. Res.: Earth Surf. 119, 1136−1154. https://doi.org/10.1002/2013JF002824.

Wang, Z., van Maren, D., Ding, P., Yang, S., van Prooijen, B., de Vet, P., Winterwerp, J., de Vriend, H., Stive, M., He, Q., 2015. Human impacts on morphodynamic thresholds in estuarine systems. Continent. Shelf Res. 111, 174−183. https://doi.org/10.1016/j.csr.2015.08.009.

Willemsen, P.W.J.M., Borsje, B.W., Hulscher, S.J.M.H., der Wal, D.V., Zhu, Z., Oteman, B., Evans, B., Moller, I., Bouma, T.J., 2018. Quantifying bed-level change at the transition of tidal flat and salt marsh: Can we understand the lateral location of the marsh edge? J. Geophys. Res.: Earth Surf. 123(10), 2509−2524. https://doi.org/10.1029/2018JF004742.

Yang, S.L., Li, H., Ysebaert, T., Bouma, T.J., Zhang, W.X., Wang, Y.Y., Li, P., Li, M., Ding, P.X., 2008. Spatial and temporal variations in sediment grain size in tidal wetlands, Yangtze Delta: On the role of physical and biotic controls. Estuar. Coast. Shelf Sci. 77(4), 657−671. https://doi.org/10.1016/j.ecss.2007.10.024.

Zhu, Q., Yang, S., Ma, Y., 2014. Intra-tidal sedimentary processes associated with combined wave−current action on an exposed erosional mudflat, southeastern Yangtze River Delta, China. Mar. Geol. 347, 95−106. https://doi.org/10.1016/j.margeo.2013.11.005.

Zhu, Q., van Prooijen, B.C., Wang, Z.B., Ma, Y.X., Yang, S.L., 2016. Bed shear stress estimation on an open intertidal flat using in situ measurements. Estuar. Coast. Shelf Sci. 182, 190−201. https://doi.org/10.1016/j.ecss.2016.08.028.

Zhu, Q., van Prooijen, B., Wang, Z., Yang, S., 2017. Bed-level changes on intertidal wetland in response to waves and tides: A case study from the Yangtze river Delta. Mar. Geol. 385, 160−172. https://doi.org/10.1016/j.margeo.2017.01.003.